Received: 25 January 2020 | Revised: 30 October 2020 | Accepted: 3 November 2020

DOI: 10.1002/ijc.33401

CANCER THERAPY AND PREVENTION

IJC International Journal of Cancer

Constitutive low expression of antiviral effectors sensitizes melanoma cells to a novel oncolytic virus

Sarah Dellac | Hamutal Ben-Dov | Ayala Raanan | Hanna Saleem | Rachel Zamostiano | Rinat Semyatich | Sara Lavi | Isaac P. Witz | Eran Bacharach | Marcelo Ehrlich

Shmunis School of Biomedicine and Cancer Research, George S. Wise Faculty of Life Sciences, Tel Aviv University, Tel Aviv, Israel

Correspondence
Eran Bacharach and Marcelo Ehrlich, Shmunis School of Biomedicine and Cancer Research, George S. Wise Faculty of Life Sciences, Tel Aviv University, Tel Aviv, Israel.
Email: eranba@tauex.tau.ac.il (E. B.) and
Email: marceloe@tauex.tau.ac.il (M. E.)

Funding information
Colton-Nadal Fund; Dr. Miriam and Sheldon G. Adelson Medical Research Foundation; Emerson Collective Cancer Research Fund; Israel Cancer Association, Grant/Award Number: 20200132; Israel Science Foundation, Grant/Award Number: 1966/18; SPARK Initative

Abstract

STAT1 is a critical effector and a target gene of interferon (IFN) signaling, and thus a central mediator of antiviral responses. As both a mediator and a target of IFN signals, STAT1 expression reports on, and determines IFN activity. Gene expression analyses of melanoma patient samples revealed varied levels of STAT1 expression, which highly correlated with expression of >700 genes. The ability of oncolytic viruses to exploit tumor-induced defects to antiviral responses suggests that oncolytic viruses may efficiently target a subset of melanomas, yet these should be defined. We modeled this scenario with murine B16F10 melanomas, immortalized skin fibroblasts as controls and a novel oncolytic virus, EHDV-TAU. In B16F10 cells, constitutive low expression of STAT1 and its target genes, which included intracellular pattern recognition receptors (PRRs), correlated with their inability to mount IFN-based antiviral responses upon EHDV-TAU challenge, and with potency of EHDV-TAU-induced oncolysis. This underexpression of interferon stimulated genes (ISGs) and PRRs, and the inability of EHDV-TAU to induce their expression, were reversed by epigenetic modifiers, suggesting epigenetic silencing as a basis for their underexpression. Despite their inability to mount IFN/STAT-based responses upon viral infection, EHDV-TAU infected B16F10 cells secreted immune-stimulatory chemokines. Accordingly, in vivo, EHDV-TAU enhanced intratumoral infiltration of cytotoxic T-cells and reduced growth of local and distant tumors. We propose that "STAT1 signatures" should guide melanoma virotherapy treatments, and that oncolytic viruses such as EHDV-TAU have the potential to exploit the cellular context of low-STAT1 tumors.

KEYWORDS
antiviral signaling, epigenetic regulation, Epizootic Hemorrhagic Disease Virus, interferon, melanoma, pattern recognition receptors, STAT1, viral oncolysis

Abbreviations: 5AC, 5-aza-2′-deoxycytidine; CI, CI-994; EHDV-TAU, Epizootic Hemorrhagic Disease Virus-Tel Aviv University; GAPDH, glyceraldehyde-3-phosphate dehydrogenase; HPRT, hypoxanthine phosphoribosyltransferase 1; IFN, interferon; ISF, immortalized skin fibroblast; ISG, interferon stimulated gene; JAK1, Janus Kinase 1; MDA5, melanoma differentiation antigen 5; MITF, Melanocyte-Inducing Transcription Factor; MLANA, Melan-A; PAMP, pathogen associated molecular pattern; PRR, pathogen recognition receptor; RIG-I, retinoic acid-inducible gene 1; S, Scriptaid; SA, SAHA; SBHA, SB; SCC, Spearmann's correlation coefficient; SKCM, Skin Cutaneous Melanoma; STAT1, signal transducer and activator of transcription 1; T, Tubacin; TCGA, The Cancer Genome Atlas; TFAP2A, transcription factor AP-2 alpha; TYR, tyrosinase; VSV, vesicular stomatitis virus.

1 | INTRODUCTION

Tumor immunoediting, a result of selective pressure applied by antitumor immunity,[1] contributes to tumor aggressiveness[2] through modified expression or function of immune mediators, down regulation of MHC class I,[3] upregulation of immune checkpoint proteins[4] or deregulation of Janus Kinase-signal transducer and activator of transcription (JAK-STAT) pathway.[5,6]

Antiviral responses initiate through recognition of pathogen associated molecular patterns (PAMPs) by pattern recognition receptors (PRRs), and are amplified via interferon (IFN)-mediated induction of antiviral genes.[7] This restricts infection in individual cells, induces antiviral state in nearby uninfected cells and stimulates systemic antiviral immunity. Such response comprises: (a) negative regulation of anabolism (eg, protein synthesis arrest), (b) induction of growth-arrest and cell death programs (eg, apoptosis, necroptosis or pyroptosis) and (c) secretion of cytokines/chemokines (eg, type I IFNs).[8,9] IFNs stimulate JAK-mediated phosphorylation of STATs, their homo- or hetero-oligomerization, nuclear translocation, and regulated expression of hundreds of interferon-stimulated genes (ISGs).[10]

Defects in IFN signaling occur in melanoma and influence tumor development,[11] metastatic progression,[12] interactions with the microenvironment,[13] escape from immune surveillance,[12] and acquired resistance to immunotherapy.[14] IFNs are employed as adjuvant therapy for high risk melanoma[15] and were proposed to inhibit melanoma growth and support melanogenesis[16] (ie, redifferentiation). IFN treatment of melanoma cells prompted identification of melanoma differentiation associated gene 5 (MDA5) as regulator of IFN-induced growth inhibition and apoptosis.[17] MDA5 is a major PRR that senses double-stranded RNA.[18] Together, this suggests that defects in IFN signaling or ISG expression may render melanoma cells more resistant to cytotoxic or cytostatic stimuli, while exposing them to viral infection.

Oncolytic virotherapy employs tailored viruses to kill cancer cells and stimulate antitumor immunity, exploiting acquired vulnerability of tumor cells to viral infections.[19,20] We selected an oncolytic clone of the Ibaraki strain of the Epizootic Hemorrhagic Disease Virus (EHDV2-IBA), a natural pathogen of ruminants, which is cytolytic and induces apoptosis, necroptosis, autophagy, and cell stress.[21] Serial passaging of EHDV2-IBA in interferon-defective human prostate cancer LNCaP cells allowed for selection of oncolytic EHDV-Tel Aviv University (EHDV-TAU). The selected virus exhibited six orders of magnitude fold increase in titer, relative to the parental virus,[5] was greatly restricted in untransformed interferon-responsive human cells,[5] and in presence of inflammatory cytokines (eg, IL-6, IFN-γ) induced oncolysis by nonproductive viral infection (ONPVI) in interferon-responsive prostate cancer cells.[22]

Here, we analyzed expression of STAT1 in melanoma databases and identified a coordinated pattern of expression of STAT1 and ISGs, PRRs and chemokines (STAT1 signature). Employing, B16F10 murine melanomas, which underexpress STAT1 and its associated genes, we characterize viral oncolysis in vitro, the epigenetic regulation of STAT1-correlated genes; and the oncolytic potential of EHDV-TAU in vivo.

What's new?

The ability of oncolytic viruses to exploit tumor-induced defects in antiviral responses suggests their potential to efficiently target definite subsets of melanomas, yet these should be defined. Here, the authors show that STAT1 is at the center of a tumor signature involving genes that mediate antiviral and immune activation responses. Using a murine melanoma model and a novel oncolytic virus, EHDV-TAU, they identify epigenetic silencing as contributing to the underexpression of antiviral genes. Moreover, they demonstrate the potential of EHDV-TAU to exploit this molecular landscape for effective oncolysis and immune stimulation.

2 | MATERIALS AND METHODS

2.1 | Drugs and reagents

JAK1 inhibitor (baricitinib, BioVision, Milpitas, California, cat. #2842), C16 (Sigma-Aldrich, St. Louis, Missouri, cat. # 60851-97-6), 5-aza-2′-deoxycytidine (Sigma-Aldrich, St. Louis, Missouri, cat. #A3656), mouse interferon β (IFN-β) (R&D Systems, Minnesota, cat. #8234-MB). The following Histone deacetylase (HDAC) inhibitors were from Sigma (cat. # EPI009) and employed at indicated concentrations: SAHA (SA; 2 μM), SBHA (SB; 2 μM), Scriptaid (S; 2 μM), CI-994 (CI, 10 μM) and Tubacin (T, 5 μM). Primers employed in this study are compiled in Supplementary Table S1. Antibodies employed throughout the study are described in Supplementary Materials.

2.2 | Virus

Generation, propagation, and purification of EHDV-TAU were previously described.[5] Generation of the VSV-Δ51M virus is described in Supplementary Methods.

2.3 | Cells

Two clones of B16-F10 (RRID:CVCL_0159) were employed: Cherry-labeled B16F10 (ChB16,[23] gift from Prof. Ronit Satchi Fainaro, Tel Aviv University) or B16F10.9 (uB16,[24] gift from Prof. Lea Eisenbach, Weizmann Institute of Science). OK (ovine kidney cells, were generated at the Kimron Veterinary Institute, Israel; and described in Reference 21), LNCaP (RRID:CVCL_0395; were from ATCC), BHK-21 (RRID:CVCL_1914, were from ATCC). Human melanoma cell lines included UCLA-SO-M12 (M12, RRID:CVCL_5T78) and YDFR (described in Reference 25). All human cell lines were authenticated (STR profiling) within the last 3 years. All experiments were performed with mycoplasma-free cells.

2.4 | Plaque assay

EHDV-TAU was collected from infected ChB16, uB16 or ISF cell cultures, released from cells by sonication and serially diluted. Plaque assay was performed as in Reference 22.

2.5 | Immunoblotting

Cell lysis, separation of 60-80 μg of protein by 10% sodium dodecyl sulfate polyacrylamide gel electrophoresis, immunoblotting and chemiluminescence detection were as in Reference 22.

2.6 | Live-dead assay

Assays were performed with LIVE/DEAD Fixable Green Dead Cell Stain Kit (cat. # L23101, Invitrogen).

2.7 | Cell proliferation assay

Cells were plated in 96-well plate (5000 cells/well; six repetitions for each time point/condition). Methylene blue assay was as in Reference 22.

2.8 | Animals

Animal care and experiments were in accordance with institutional guidelines of Tel Aviv University and were approved by the Institutional Animal Care and Use Committee, George S. Wise Faculty of Life Sciences, Tel Aviv University. C57BL/6J mice were purchased from the institutional breeding colony, originated from C57BL/6J from The Jackson Laboratory.

2.9 | In vivo tumor models

ChB16 cells (2×10^6 cells/100 μL) were injected to the right (single tumor experiments), or right and left of the spine (double tumor experiments), ensuring subcutaneous bleb formed distinctly apart from one another. Tumor growth was measured every 1-3 days using calipers, and volume was calculated by the formula width $^2 \times$ length $\times$ 0.52. After reaching palpable size (~5-10 mm^3), mice were administered 3-4 intratumoral injections (EHDV-TAU or PBS, every 4-5 days). Initial dose was of 10^8 pfu in 30-50 μL dose/mouse, while subsequent doses increased according to tumor volume (eg, 2-fold). Mice were either grown until their tumor(s) reached 1000 mm^3 (for survival assays) or until a specific point used for tumor harvest and dissociation. In experiments involving mice with two contra-lateral tumors, only the right-flank tumor was injected with either EHDV-TAU or PBS (control), while the left-flank tumor remained untouched.

2.10 | Analysis of The Cancer Genome Atlas databases

Calculations of correlation in gene expression or β-score of promoter methylation were carried out with cBioPortal (PanCancer Atlas, comprising 448 samples).[26] Stratification of samples or calculation of Kaplan-Meier plots according to normalized gene expression values (from The Cancer Genome Atlas database of Skin Cutaneous Melanoma [TCGA SKCM]) was with UCSC Xena Genome Browser.[27]

2.11 | Statistical analyses

Data are expressed as mean ± SE. Statistical significance was assessed by Student's *t*-test (two-tailed, unless stated otherwise) or two-tailed ANOVA. A value of $P \leq .05$ was considered significant. in vitro experiments were done in triplicates from three independent experiments or six repeats from two independent experiments (unless stated otherwise). in vivo experiments were done with at least three mice per experiment in at least 2-3 independent experiments using independent litters between experiments. *P* values are indicated as $^*P < .05$; $^{**}P < .01$; $^{***}P < .001$; $^{****}P < .0001$.

2.12 | Supplementary methods

The supplementary methods section describes the production and stimulation of Bone-Marrow Derived Macrophages (BMDM), the employment of cytokine arrays, the generation of the oncolytic mutant of the vesicular stomatitis virus (VSV-Δ51M), and the fluorescence microscopy procedures.

3 | RESULTS

3.1 | Differential expression of STAT1 and STAT1-correlated genes in melanoma

STAT1 is unique as it is both a target gene and a mediator of JAK/STAT signaling. Therefore, we queried TCGA SKCM,[28] employing cBioPortal (PanCancer Atlas,[26] comprising 448 samples) for identification of genes coexpressed with STAT1 (Spearman's correlation coefficient [SCC] values ≥0.5, Supplementary Table S2). Of the 702 genes fitting this definition, 384 (53.3%) were also identified as STAT1 targets in Chip-Seq studies (Encode project[29]). For visualization of coexpression tendencies, we ranked the 30 genes presenting highest SCC values (with UCSC Xena Browser,[27] $0.88 \geq SCC \geq 0.77$, $E{-}125 < P < E{-}74$; Figure 1A). We next calculated (with UCSC Xena

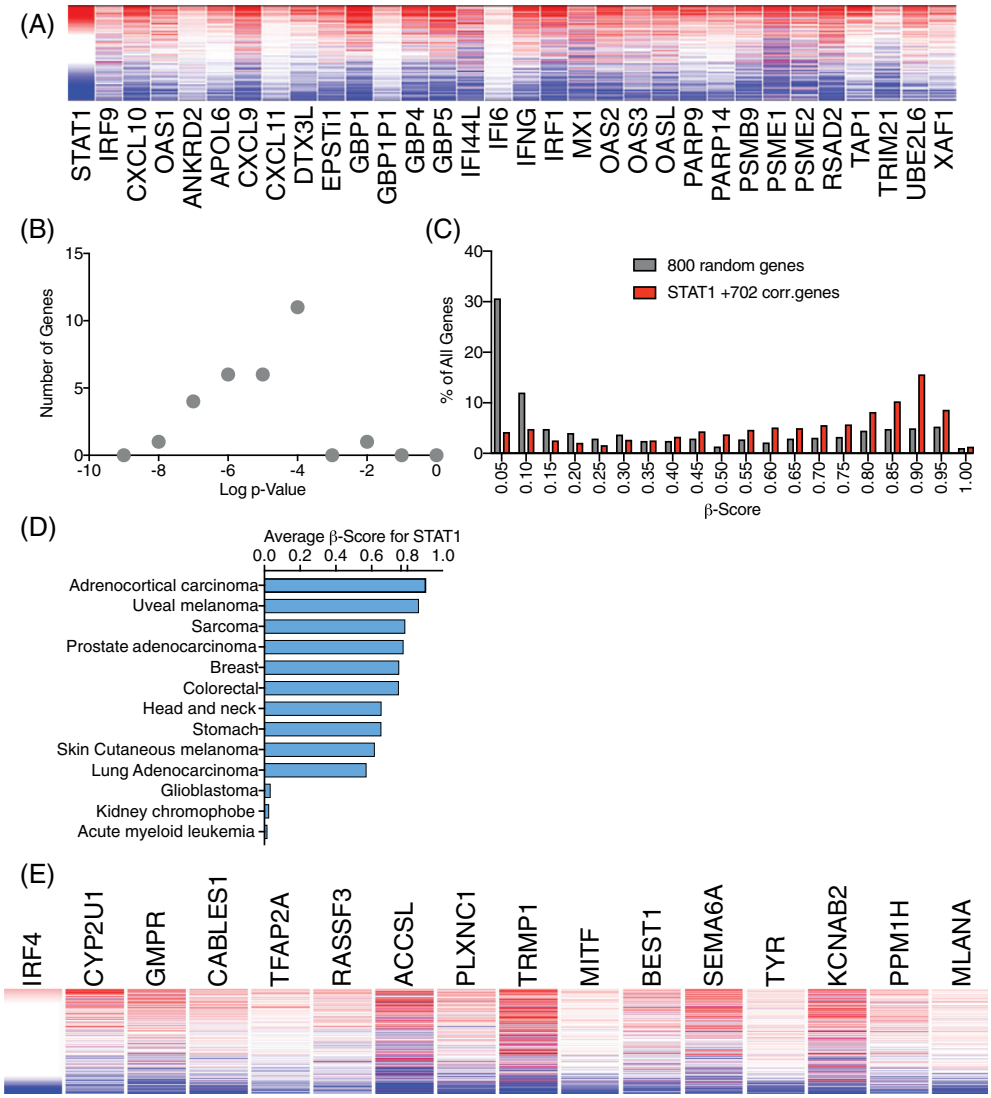

FIGURE 1 STAT1-correlated gene expression patterns in a patient-derived melanoma dataset. TCGA SKCM PanCancer Atlas database analysis was carried with cBioPortal[26] for selection of 702 genes presenting Spearman's correlation ≥0.5 with STAT1 expression, or calculation of β-score of promoter methylation; or with the UCSC Xena Genome Browser[27] for stratification of samples, or calculation of Kaplan-Meier survival plot (according to log2(norm_count+1) gene expression values). A, Samples from TGCA SKCM database (each horizontal line represents a single sample) were stratified according to STAT1 expression (red, white and blue colors are indicative of high, medium and low normalized gene expression values, respectively, for each indicated gene). B, Graph depicts the number of genes (out of 31 from A) presenting an indicated p value for differences in survival between high and low expressers. For all genes in A, lower expression correlated with decreased survival. C, Graph depicts the distribution of percentage of genes, from either 800 randomly selected human genes, C, or STAT1 and 702 genes with coordinated expression with STAT1, with the β-score values (indicative of promoter methylation) within indicated ranges. Higher β-score values indicate higher methylation values. D, Average β score values for STAT1 in indicated tumors types. E, Stratification of expression of melanogenesis markers in samples from TGCA SKCM database, according to IRF4 log2(norm_count+1) expression values (color coding as in A)

Browser) Kaplan-Meyer survival curves associated with differential expression of these genes. This revealed that decreased expression of STAT1, or of any of these 30 genes, was significantly associated with worsened prognosis (distribution of *P* values is presented in Figure 1B). To gain insights into the molecular underpinnings of this correlated gene expression pattern, we queried the TCGA SKCM database for promoter methylation of STAT1 or of the 702 STAT1-correlated genes, or of 800 randomly sampled genes from the human genome. This revealed significantly higher methylation of promoters of STAT1-correlated genes (*P* = 1.1E−52, Figure 1C). Querying the TCGA database for STAT1 promoter methylation across cancer types revealed an overall tendency of high values (ie, high methylation), with few exceptions (eg, glioblastoma, Figure 1D); suggesting that STAT1 may be under similar regulation in different tumor types. Together, these data suggest: (a) correlated expression in melanoma of STAT1 and its target genes, (b) association of low STAT1 expression (or of genes correlated with STAT1) with reduced survival in melanoma, and (c) a putative role for epigenetic mechanisms in

regulating the expression of STAT1 and its associated genes in a subset of melanomas. As expected, gene ontology analysis (with PANTHER[30]) revealed enrichment for immune regulatory and antiviral genes among the STAT1-correlated genes in melanoma (Supplementary Table S3). IFN, which regulates expression of STAT1 and ISGs via JAK/STAT signaling, was proposed to reduce the tumorigenic potential of melanoma via promotion of melanogenesis and redifferentiation of melanoma cells.[16] To probe if expression of STAT1 correlated with that of melanogenesis markers (eg, MITF, MLANA, TYR, TFAP2A) we examined their coexpression in the TCGA SKCM database (visualized, with UCSC Xena Browser, Figure 1E). Among themselves, markers of melanocyte differentiation were coexpressed (SCC > 0.5, $P < E{-}22$, for all gene pairs). However, these genes lacked correlation with STAT1 expression (SCC < 0.05), or with the interferon-induced marker of melanosome differentiation (MDA5,[17] SCC < 0.02). Together, this suggests that canonical IFN/JAK/STAT signaling and ISG expression may not be directly associated with differentiation/de-differentiation of melanoma. However, expression of melanogenesis markers was highly correlated with expression of the interferon regulated factor 4 (IRF4, SCC > 0.53, $P < E{-}25$, Figure 1E), suggesting the association of melanoma differentiation/de-differentiation with the noncanonical interferon regulated factor IRF4 (as in Reference 31). Together, our analysis suggests that a subpopulation of melanoma patients presenting lower

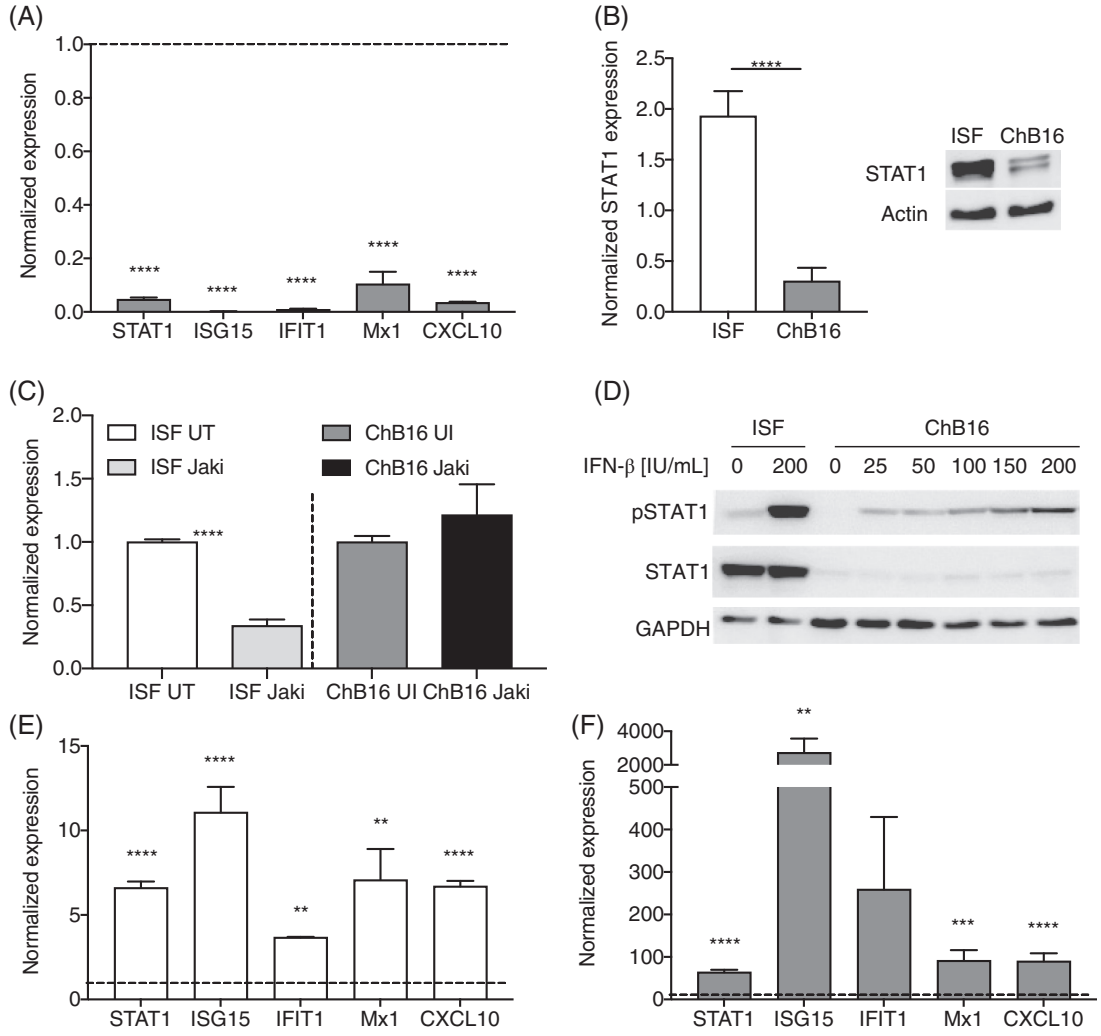

FIGURE 2 Both ISF and ChB16 cells are interferon-responsive, but differ in constitutive ISGs levels. A, qRT-PCR analysis of ISGs expression levels in naïve ISF and ChB16 cells. Graph depicts relative expression (levels in ISF cells are taken as 1 and shown as dashed line) of the indicated ISGs (n = 6). B, Immunoblot analysis of STAT1 expression in naïve ISF and ChB16. Right panel represents a typical blot; left panel shows densitometry analyses (n = 5). C, qRT-PCR analysis of STAT1 expression in naïve (UT) or baricitinib (JAK inhibitor, Jaki)-treated ISF or ChB16 cells (1 μM, 15 hours). Graph depicts relative expression levels (levels in untreated cells, UT, of each cell type are taken as 1). D, Immunoblot analysis of dose-dependent response to IFN-β stimuli in ChB16 cells. E and F, qRT-PCR analysis of ISG expression levels following stimulation with IFN-β (200 U/mL, 15 hours). Graphs depicts relative expression levels in ISF, E, and ChB16, F, cells. Expression in naïve cells (of each cell type) was taken as 1 and is shown as dashed lines (n = 6). Of note, while marked increases were observed in ChB16 following IFN-β stimuli, absolute expression levels of indicated genes (gene of interest/housekeeping gene) still remained lower (by 2-5-fold) than those in ISF cells

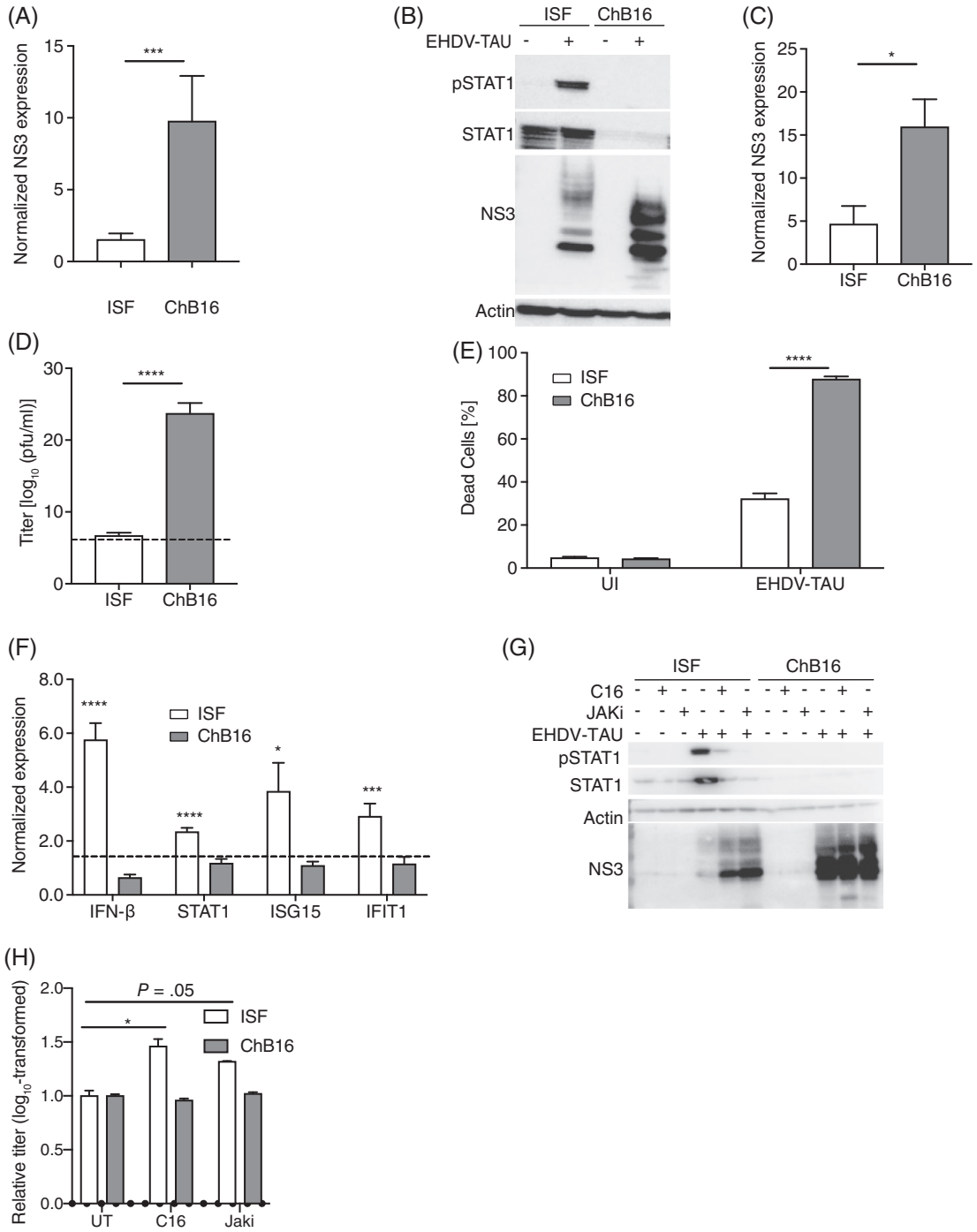

FIGURE 3 EHDV-TAU infects and kills ChB16 cells more efficiently than ISF cells. A, ISF or ChB16 cells were infected with EHDV-TAU (12 hours, MOI = 1). Graph depicts expression of the EHDV-TAU nonstructural protein 3 (NS3) mRNA normalized to hypoxanthine phosphoribosyltranferase (HPRT) in ISF or ChB16 cells (n = 4). B, ISF and ChB16 cells were infected or not with EHDV-TAU (24 hours, MOI = 1). Cell lysates were immunoblotted for pSTAT1, STAT1, NS3 or Actin (as loading control). C, Graph depicts densitometry quantification of NS3 expression normalized to actin (n = 7). D, ISF and ChB16 cells were infected or not with EHDV-TAU (48 hours, MOI = 1). Cells and culture supernatant were collected and processed for plaque assay assessment of viral titer. Graph shows calculated titers (n = 6). Titer of inoculum is presented as dashed line. E, Cells were infected (EHDV-TAU, 48h, MOI = 1) or not (UI). Cell death was assessed with LIVE/DEAD Fixable Stains for flow cytometry. Graph depicts percentage of dead cells in indicated conditions (n = 3). F, ISF and ChB16 were infected or not with EHDV-TAU (MOI = 1, 12 hours). Expression of indicated genes was measured by qRT-PCR (n = 6). Graph depicts relative expression levels of IFN-β, STAT1 or ISGs (ISG15 or IFIT1) in infected cells. Expression levels in uninfected cells of each cell type are taken as = 1, and shown as dashed line. G, ISF or ChB16 cells were pretreated (or not) with either baricitinib (JAKi, 0.5 μM) or the PKR-inhibitor (C16, 1 μM) for 3 hours, followed by infection (or not) with EHDV-TAU (48 hours, MOI = 0.5, in same conditions as pretreatment). H, Graph depicts relative $\log_{10}$-transformed titers in indicated conditions. *, $P < .05$, one tailed Student's *t*-test, also employed for calculation of $P = .05$ in ISF-JAKi condition

expression of STAT1 and its correlated genes may also present hampered antiviral responses and thus be a good target for oncolytic virotherapy.

3.2 | Absence of constitutive JAK-mediated ISG expression in murine melanoma model

To extend our study, we employed murine B16F10 melanoma cells, labeled with mCherry (ChB16, Cherry-labeled B16F10). This model allows for in vivo viral oncolysis studies in immune-competent C57BL6 mice, is extensively employed in immuno- and virotherapy studies, and the mCherry marker is useful for cell separation. As control, we employed immortalized C57BL6 skin fibroblasts (termed hereafter ISFs). Initially, we compared the expression of STAT1 or ISGs in unstimulated/uninfected ChB16 and ISF cells (ie, constitutive expression). This analysis revealed markedly lower expression of STAT1 and ISGs in ChB16 cells, shown here at the mRNA (Figure 2A) and protein (Figure 2B) levels. To test if constitutive JAK/STAT signaling contributes to the observed differences, we treated cells with baricitinib (JAK inhibitor). This revealed a baricitinib-mediated decrease in STAT1 expression exclusively in ISF cells (Figure 2C). To test if this reflects an inability of ChB16 cells to respond to IFN stimuli, we treated ISF or ChB16 cells with IFN-β and measured STAT1 phosphorylation (Figure 2D) or STAT1/ISG expression (Figure 2E,F); revealing IFN-β-induced responses in both cell types. Together, our data show that while both ChB16 and ISF cells respond to IFN-β stimuli, they differ in constitutive expression of JAK/STAT target genes, present in ISF and lacking in ChB16 cells.

3.3 | EHDV-TAU infects and kills B16F10 melanoma cells with dependence on lack of IFN signaling

To probe if the differences in constitutive JAK-mediated expression of STAT1/ISGs translates into differential sensitivity to viral infection, we challenged ChB16 cells or ISF cells with oncolytic EHDV-TAU, as this virus was selected to exploit interferon deficiencies in cancer cells.[5] EHDV-TAU-infected ChB16 cells expressed higher levels of the nonstructural viral protein 3 (NS3 mRNA, Figure 3A; NS3 protein, Figure 3B,C). Moreover, and unlike control cells, ChB16 cells supported marked increases in viral titer (48 hpi, 3D). FACS-based assessment of the percentage of dead cells revealed enhanced susceptibility of ChB16 cells to EHDV-TAU-mediated oncolysis, relative to ISF cells (Figure 3E).

Next, we measured the ability of EHDV-TAU to activate JAK/STAT signaling in these cell types. This revealed EHDV-TAU-mediated increases in STAT1 phosphorylation exclusively in ISF cells (Figure 3B). Moreover, EHDV-TAU failed to induce expression of IFN-β, STAT1 or ISGs (ISG15 or IFIT1) in ChB16 cells, in sharp contrast to significant increases that were observed in ISF cells (Figure 3F). To test if JAK/STAT signaling restricts EHDV-TAU infection in ISF cells, we treated cells with inhibitors of JAK or of the double stranded RNA kinase PKR (an ISG and negative regulator of reovirus-mediated oncolysis[19]). In ISF cells, such treatments reduced EHDV-TAU-induced phosphorylation of STAT1 (Figure 3G), increased expression of the NS3 protein (Figure 3G) and production of infectious virions (Figure 3H); indicating the involvement of JAK-mediated signaling and PKR in anti-EHDV-TAU responses. In ChB16 cells, EHDV-TAU infection was not affected by either inhibitor (Figure 3G,H). Pretreatment of ChB16 with IFN-β, prior to EHDV-TAU infection, resulted in: marked decreases in production of viral NS3 mRNA (Figure 4A) and protein (Figure 4B,F) and more than 10 orders of magnitude reduction in virus production (Figure 4C). IFN-β also restricted infection in ISF cells (Figure 4A-C). Importantly, pretreatment with IFN-β was cytoprotective in both cell types (Figure 4D,E). Prolonged treatment of ChB16 cells with IFN-β also resulted in increased STAT1 protein, also when combined with EHDV-TAU (Figure 4F). These results suggest that ChB16 respond to IFN, but fail to raise IFN-based antiviral responses upon EHDV-TAU challenge. Given the phenotypic diversity among different B16F10 sublines,[32] we employed an additional B16F10 isolate (B16F10.9, uB16) and compared ChB16 and uB16 for IFN response and infection-related parameters. Basal expression of STAT1 protein, and phosphorylation of STAT1 following IFN-β stimulation were higher in uB16 (Supplementary Figure S1A). Following EHDV-TAU infection, uB16 cells produced intermediary levels of NS3 (ChB16 > uB16 > ISF), activated JAK/STAT signaling (Supplementary Figure S1B), increased expression of IFN-β, STAT1 and of ISGs (Supplementary Figure S1C) all in contrast to ChB16, and produced infective EHDV-TAU virions at intermediary titer when compared to ISF cells (low) or ChB16 cells (high) (Supplementary Figure S1D). Moreover, while induction of cell death at 24 hpi was exclusively observed in ChB16 cells, cell death was indistinguishable between ChB16 and uB16 at 48 hpi (Supplementary Figure S1E). These data suggest that in contrast to ChB16 cells, uB16 are capable of viral sensing and activation of IFN-based antiviral signaling upon exposure to EHDV-TAU. This signaling reduces but does not prevent EHDV-TAU infection, and retards but does not prevent EHDV-TAU mediated oncolysis. To extend our analysis to human melanoma cells we initially compared UCLA-SO-M12 (M12) and YDFR cells by querying the recently published proteome of these cells.[33] This revealed significant differences in expression of STAT1 (YDFR > M12) and of a subset of the STAT-correlated genes (50 were detected, 28 presented higher expression in YDFR cells and 10 exhibited increased expression in M12 cells; Supplementary Table S4); suggesting that M12 cells conform more with the a "low-STAT1-signature" profile. Immunoblot analysis revealed higher STAT1 expression in YDFR cells, and upon infection with EHDV-TAU we observed differences in NS3 expression (YDFR $\ll$ M12), virus titer (YDFR < M12) and STAT1 activation (YDFR > M12) (Supplementary Figure S2). Pretreatment with a JAK inhibitor (baricitinib) increased the percentage of infected YDFR cells (Supplementary Figure S2); supporting the notion of JAK/STAT-mediated restriction of EHDV-TAU infection in this cell

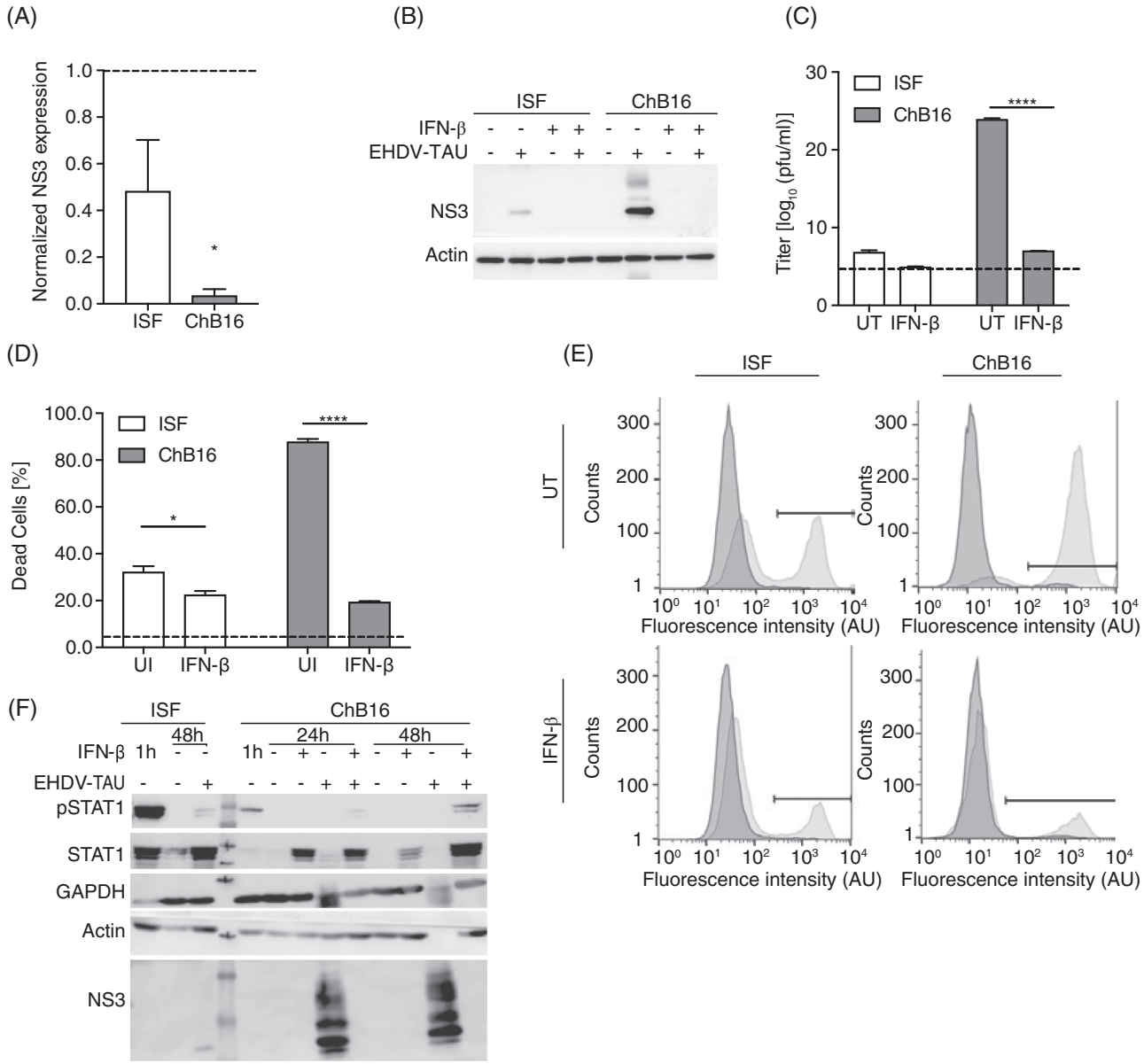

FIGURE 4 IFN-β inhibits EHDV-TAU infection and is cytoprotective. A, ISF or ChB16 were treated (or not) with IFN-β (200 U/mL, 3 hours) and infected with EHDV-TAU (MOI = 1, 12 hours). Graph depicts qRT-PCR assessment of HPRT-normalized expression levels of NS3 (levels in samples of each cell type without IFN-β are taken as = 1 and presented as dashed line, n = 4). B, ISF or ChB16 were treated (or not) with IFN-β (200 U/mL, 4 hours) and infected (or not) with EHDV-TAU (MOI = 1, 24 hours). Panel depicts immunoblot analysis of NS3 and Actin expression in the indicated conditions. C, ISF or ChB16 were treated (or not) with IFN-β (200 U/mL, 4 hours) and infected with EHDV-TAU (MOI = 1, 48 hours). Production of infectious virions was measured by plaque assays. Titer of inoculum is indicated by dashed line (n = 3). D and E, Cells were infected as in C. Viability of uninfected (dark grey) or infected (light grey) cells was measured by fluorescence intensity (right shift is indicative of death). In D, graph depicts the average (±SE) percentage of cell death in indicated conditions (n = 3). F, ChB16 or ISF cells were treated or not with IFN-β (200 U/mL, for either 1 hours, as indicated; or for a pretreatment of 6 hours followed by the indicated time period of infection), and infected (or not) with EHDV-TAU (MOI = 0.1, for 24 or 48 hours). Immunoblot is representative of independent repeats (n = 3)

type. EHDV-TAU infection resulted in readily detectable caspase 3 activation in M12 cells, and in a reduction in cell viability in both cell types, supporting the notion of its oncolytic potential.

To examine if the effects we observed with EHDV-TAU are specific for this oncolytic virus, we generated an oncolytic version of the vesicular stomatitis virus (VSV,[20]), in which methionine 51 of the M protein was deleted (VSV-Δ51M); and infected ISF, uB16 and ChB16 cells. Infection with VSV-Δ51M (24 hours, MOI = 1) differed among the cell types (ChB16 > uB16 > ISF; measured by expression of VSV protein G or M gene, Supplementary Figure S3), while inducing phosphorylation and expression of STAT1 in both B16F10 cell types. This activation sharply contrasted with the lack of STAT1 activation in VSV-Δ51M-infected ISF cells, most probably due to absence of infection. These results underscore the cell-type and virus-specificity of oncolytic-virus-cancer cell interactions. The lack of JAK/STAT signaling activation in ChB16 cells by EHDV-TAU, contrasts with such

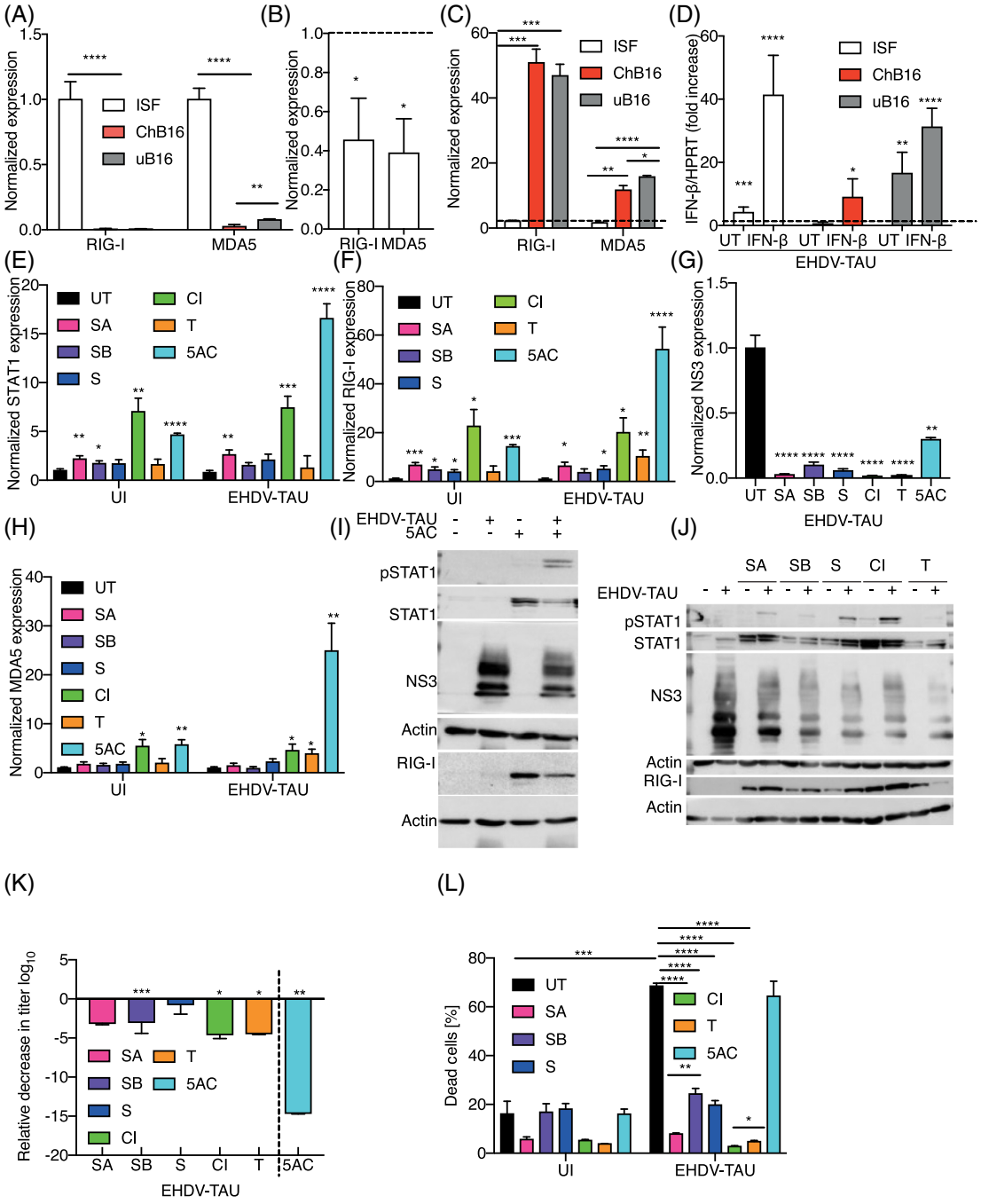

FIGURE 5 Differential regulation of PRR expression in ISF, ChB16 and uB16 cells. A, The expression of RIG-I and MDA5 was measured by qRT-PCR in uninfected and unstimulated ISF, ChB16, or uB16 cells. Graph depicts levels of expression relative to expression in ISF cells (taken as 1 and indicated with dashed line). B, Relative expression level of RIG-I and MDA5 in ISF cells treated (or not) with JAK-inhibitor (1 μg/mL, 24 hours). Dashed line marks expression levels in untreated cells (taken as 1). C, Graph depicts expression of RIG-I or MDA5 in ISF, ChB16 and uB16 cells following IFN-β stimulation (200 U/mL, 16 hours). To facilitate comparison of levels between cell types, expression was normalized to level of unstimulated cells taken as 1 (dashed line). D, ISF, ChB16 or uB16 were pretreated or not with IFN-β (200 U/mL, 3 hours) and infected or not with EHDV-TAU (12h, MOI=1). Expression of IFN-β was measured by qRT-PCR (n = 3). All bars in graph refer to infected cells, while, dashed line represents expression in untreated/uninfected cells (taken as 1). E-H, ChB16 cells, pretreated (or not) for 24 hours with different HDAC inhibitors or 5AC and were infected (or not) with EHDV-TAU (24 hours, MOI = 1; n = 3) in same conditions as pretreatment. Abbreviations appearing in the graph are: UT, untreated; SA, SAHA; SB, SBHA, S, Scriptaid; CI, CI-994; T, Tubacin; and 5AC, 5-aza-2′-deoxycytidine. Graphs depict gene expression of STAT1, E, RIG-I, F, MDA5, H or NS3, G, measured by qRT-PCR. I and J, Immunoblot analysis of pSTAT1, STAT1, NS3, RIG-I and Actin in ChB16 cells, pretreated (or not) with 5AC, I or HDAC inhibitors, J, and infected or not with EHDV-TAU (24 hours, MOI = 1). K and L, ChB16 cells were pretreated (or not) with epigenetic modifiers (for 24 hours), and infected (or not) with EHDV-TAU (MOI = 1, 48 hours). Production of infectious virions was measured by plaque assay. Graph depicts the reduction in viral titer upon different treatments (K, titer in untreated cells is taken as 1; n = 3). Dotted vertical line indicates that viral titer with 5AC was measured and compared to untreated cells in a separate series of experiments. L, Graph depicts the average percentage of dead cells in indicated conditions (n = 3)

activation by VSV-Δ51M, potentially highlighting unique features of EHDV-TAU in exploiting cancer-related defects to antiviral responses.

3.4 | Low expression of PRR and defective viral sensing in ChB16 cells

Based on the role of PRRs in igniting IFN antiviral responses, and on their varied and highly correlated expression in patient-derived samples across multiple cancer types including melanoma (Supplementary Figure S4), we hypothesized that the impaired response of ChB16 to EHDV-TAU may be a result of low expression of cytoplasmic dsRNA sensors (eg, RIG-I or MDA-5). Assessment expression of these PRRs in ChB16, uB16 or ISF cells (by qRT-PCR) revealed significantly higher levels of expression in ISF cells (Figure 5A). Comparison of expression in ChB16 vs uB16 revealed mild but significantly higher levels in uB16 (Figure 5A). Treatment of ISF cells with JAK inhibitor significantly reduced expression of STAT1, RIG-I or MDA5 (Figure 5B), suggesting that their basal expression depends on constitutive JAK/STAT signaling. Treatment of ISF, ChB16 or uB16 cells with IFN-β increased expression of RIG-I and MDA-5 in all three cell types (Figure 5C), suggesting that these genes are responsive to IFN-β in all three cell types. Given that IFN-β gene induction is a direct result of viral sensing, we tested the induction of IFN-β gene upon EHDV-TAU infection. While ISF and uB16 cells raised IFN-β gene expression upon infection, ChB16 cells failed to do so (Figure 5D, UT samples). We next tested the ability of pretreatment with exogenous IFN-β ligand, to promote sensing of EHDV-TAU in ChB16 cells. Indeed, pretreated ChB16 cells elevated the expression of IFN-β upon EHDV-TAU challenge (Figure 5D), implying that minimal expression of PRRs in ChB16 results in their inability to sense EHDV-TAU.

3.5 | Epigenetic regulation of PRR expression in ChB16 cells

Based on the tendency toward promoter methylation of STAT1-related genes in melanoma patients (Figure 1C), and on the increased immunogenicity of melanoma cells treated with histone deacetylase inhibitors (HDACis),[34] we hypothesized that expression of PRRs may be epigenetically suppressed in ChB16 cells. To test this hypothesis, we treated (or not) ChB16 cells with multiple different HDACis (indicated in Figure 5 Legend) or with the DNA methyltransferase inhibitor 5-aza-2′-deoxycytidine (5AC), infected (or not) such cells with EHDV-TAU and measured STAT1, RIG-I, MDA-5 or NS3 gene expression (Figure 5E-H); or protein expression (Figure 5I-J). Such analyses revealed epigenetic-modifier-induced increases in expression of the STAT1, MDA-5 or RIG-I (with differential effects of distinct HDACis); and further increases upon EHDV-TAU infection of 5AC-treated cells (Figure 5E,F,H). Notably, NS3 expression was reduced by either HDACi or 5AC treatment (Figure 5G). At the protein level, epigenetic modifiers increased expression of STAT1 and restored STAT1 phosphorylation and RIG-I expression, while reducing NS3 protein levels (Figure 5I-J). Accordingly, epigenetic modifiers also reduced viral titers (Figure 5K). Notably, while HDACs were cytoprotective upon EHDV-TAU infection, the EHDV-TAU-5AC combination retained its full cell killing potential (Figure 5L). Similarly, combined treatment of human melanoma cells with EHDV-TAU and 5AC resulted in reduced infection, while retaining the cell killing potential of EHDV-TAU (Supplementary Figure S5). In contrast, VSV-Δ51M infection of ChB16 cells treated with 5AC, resulted in markedly reduced cell death levels (in addition to attenuation of infection, Supplementary Figure S5). Together, these data support the notions of epigenetic silencing of STAT1 and PRRs in melanoma and of the differential potential of distinct oncolytic viruses (eg, EHDV-TAU or VSV-Δ51M to explore such altered gene regulation in different therapy scenarios (eg, with or without combined 5AC treatment).

3.6 | Immune stimulation by EHDV-TAU

The lack of an IFN-β-based autocrine antiviral signaling loop in ChB16 cells infected with EHDV-TAU raised the possibility that such oncolytic-virus-cancer-cell combination will fail to secrete activators of immune cells. However, cytokine-array-based assessment of the secretome of infected or uninfected ChB16 cells revealed EHDV-TAU-stimulated secretion of CXCL1, CXCL2 and CXCL10 (Figure 6A). Furthermore, conditioned media of EHDV-TAU-infected B16F10 cells activated ISG transcription in bone marrow derived macrophages of C57BL/6 mice (Figure 6B). Given that no STAT1 activation is observed in EHDV-TAU-infected ChB16 cells, and all interferons activate STAT1, we propose that additional EHDV-TAU-induced ligands may mediate such effects. To test the oncolytic and immunostimulatory potentials of EHDV-TAU in vivo, we grafted ChB16 cells onto C57BL/6 mice, and injected palpable tumors with either EHDV-TAU or PBS (as control; Figure 6D,6E). A significant decrease in tumor growth of the EHDV-TAU-treated tumors as compared with those injected with PBS was observed (Figure 6D). Analogous experiments performed with uB16 cells, also revealed significant reduction in volume of EHDV-TAU-injected tumor as compared to PBS-injected tumors (Supplementary Figure S1F). To test for potential effects of EHDV-TAU on distant tumors we grafted ChB16 tumors on either side of the spine (double-tumor model 6C, Figure 6E-F). Once palpable, right side tumors were intratumorally injected with EHDV-TAU or PBS. EHDV-TAU significantly reduced the growth of both the proximal (directly treated, 6E) and distal (Figure 6F) tumors, suggesting that EHDV-TAU-based oncolytic virotherapy induces both local and systemic effects. Importantly, EHDV-TAU treatment of mice of the double-tumor mode, significantly enhanced survival (Figure 6G). To further understand the effect of EHDV-TAU on antitumor immunity, we harvested PBS- or EHDV-TAU-injected tumors, processed them into single-cell suspensions and stained for various leukocyte markers (Figure 6I). No significant differences, between EHDV-TAU- or PBS-treated tumors, were observed in the percentages of neutrophils, T-helper cells, macrophages, dendritic cells, and natural killer cells. However,

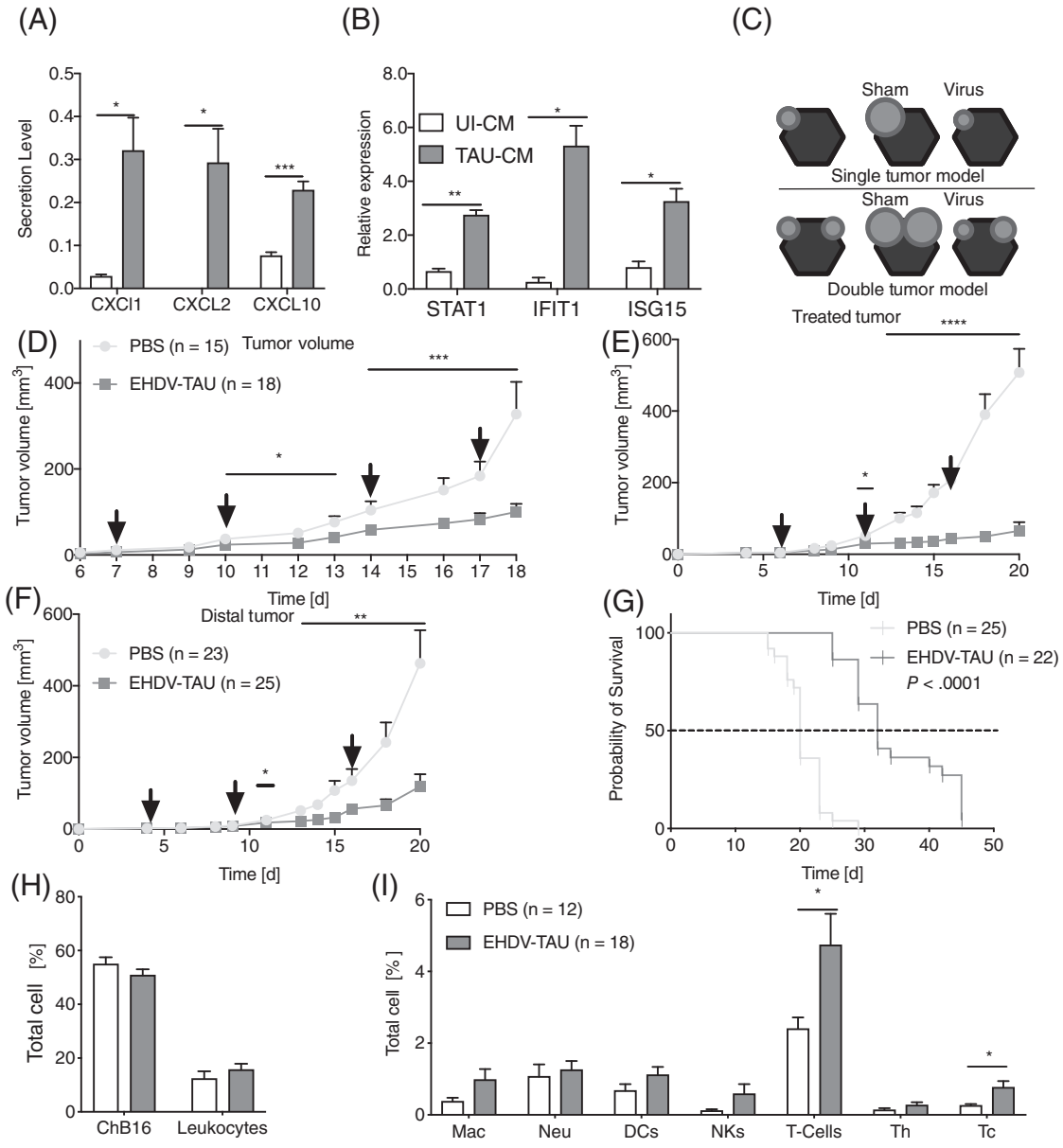

FIGURE 6 EHDV-TAU-infected ChB16 cells secrete immune-attractant chemokines and induce immunostimulation. A, ChB16 cells were infected (or not) with EHDV-TAU (MOI = 0.1, 24 hours), after which medium was replaced by 0.5% serum-containing media for 12 hours. Collected media were employed to probe cytokine array membrane. Graph depicts densitometry quantification of two independent experiments (four measurements per/cytokine). B, Bone-marrow derived macrophages (BMDMs) of C57BL/6 mice were incubated for 12 hours with filtered-conditioned media of uninfected (UI-CM) or infected (TAU-CM) B16F10 cells. Exposure to conditioned media resulted in upregulation of immune mediators (STAT1, IFIT1 and ISG15) in BMDMs as measured by qRT-PCR. C, Schematic depiction of experimental setup. C57BL/6 mice (6-8 weeks old) were injected subcutaneously with 2×10^6 ChB16 cells to the right lower back (top panel, single tumor model) or to both right and left sides of the spine, with at least 1.0 cm between forming subcutaneous blebs (bottom panel, double tumor model). Following appearance of palpable tumors, mice received intratumoral injections of equal volume of PBS (control) or EHDV-TAU (ranging from 10^8-2×10^{10} pfu/dose in PBS; according to tumor volume). Tumor volumes were measured at indicated time points. Treatments were administered, at the arrow-indicated time points. D, Graph depicts tumor growth of single-tumors receiving PBS (n = 15) or EHDV-TAU (n = 18). E and F, Graphs depict the growth of the treated, E, and untreated, F, tumors of tumor-bearing mice in the double-tumor model (see C bottom panel) receiving PBS (n = 23) or EHDV-TAU (n = 25) treatments. G, Graph depicts the survival of mice from experiment in E and F. Of note, no significant differences in mouse weight were observed between the treatment groups, indicative of lack of EHDV-TAU-induced detrimental health effects. H and I, Single tumors were harvested 20 days after ChB16 injection, and 2 days after 4th injection with PBS (n = 15) or EHDV-TAU (n = 18), dissociated to single cells, and stained for various leukocyte markers. Cells were then fixed in 2% PFA and sorted by FACS, using a Flow cytometer S100EXi (Stratagim, San Jose, CA, USA). Graphs depict the indicated cell population as percentage of the total cell suspension. Abbreviations (marker): B16 = ChB16 (mCherry); Leu = leukocytes (CD45); Mac = macrophages (F4/80); Neu = neutrophils (Ly6G); DCs = dendritic cells (CD11c); NKs = natural killer cells (NK1.1); T-Cells (CD3); Th = T-helper cells (CD3 and CD4); Tc = T-cytotoxic cells (CD3 and CD8). All leukocytes were gated from mCherry-negative population and CD3 positive (for T-cells, Th, Tc) or CD45 (for all others)-positive cells. FACS analysis was done with FlowJo v10

CD3-positive cells were significantly higher in EHDV-TAU-treated tumors, and more specifically, such infected tumors exhibited higher percentages of T-cytotoxic cells (double-positive for CD3 and CD8, Figure 6I).

4 | DISCUSSION

Oncolytic viruses, including EHDV-TAU, exploit tumor-induced defects to cell autonomous immunity to specifically infect and kill cancer cells.[5,22,35] The various manners by which cancers modify cell autonomous immunity, and the heterogeneity among viruses, raise the prospect of matching viruses and tumor types; improving in this manner oncolytic virotherapy through better patient stratification and novel combination therapy strategies. Previously, we identified defects to JAK1 expression, in a subset of prostate cancer cells, as the basis for their interferon insensitivity and inability to mount antiviral responses (eg, anti-EHDV-TAU).[5,22] Of note, the FDA-approved oncolytic virus (T-VEC) is for melanoma[36]; raising the questions of how are antiviral responses in melanomas hampered, and how can these defects be exploited in therapy settings.

Here we show that in human melanoma samples, STAT1 is at the center of a signature involving genes that mediate antiviral and immune-activation responses. This is in accord with STAT1 being both a crucial mediator of JAK/STAT signaling[37] and an ISG[38]; thus executing and reporting on IFN/JAK/STAT signaling. STAT1-signature genes showed higher promoter methylation than randomly-selected human genes; suggesting epigenetic regulation as putative basis for coordinated expression. Decreased expression of STAT1-signature genes was associated with decreased survival of melanoma patients; suggesting that STAT-related functions (eg, interactions with the immune tumor microenvironment) are of clinical importance. Visualization of per-patient expression levels of RIG-I and MDA-5 in different cancer types of the TCGA revealed varied expression between patients of given tumor types (>10-fold for the majority of cancer types, and >50-fold in melanoma, Supplementary Figure S4, in addition to a tendency of low and highly-correlated normalized expression (Supplementary Figure S4). This suggests that tumors may differ in intracellular viral-RNA recognition and its ensuing antiviral responses,[39] and that subsets of patients of many tumor types, presenting low PRR expression, may be good candidates for oncolytic virotherapy. In this context, nucleotide sensing by RIG-I and MDA-5 may play important roles in cancer development or therapy. Thus, dsRNA or 5′-triphosphate RNA oligonucleotides, which activate MDA-5 or RIG-I respectively,[39] were employed to stimulate proapoptotic signaling and/or immunogenic cell death in different cancer models.[40,41] Moreover, RIG-I activation is critical for effective CTLA-4-based checkpoint blockade,[42] and enhanced sensing of dsRNA by cancer cells, overcomes resistance to immune checkpoint blockade.[43] Notably, Reoviruses are recognized by both MDA-5 and RIG-I,[44] establishing their strong potential for immune-activation. We propose that oncolytic viruses of the Reoviridae (eg, EHDV-TAU) can promote a therapeutically advantageous "T-cell inflamed" tumor microenvironment[45] through activation of PRRs and stimulated-secretion of inflammatory cytokines.

B16F10 cells, and in particular the ChB16 subline, emulate the subset of melanomas with low STAT1, RIG-I and MDA-5 expression. These cells failed to raise anti-EHDV-TAU responses. This contrasted with ISF or uB16 cells, which responded to EHDV-TAU by activating IFN/JAK/STAT signaling. ISF cells, which expressed highest levels of STAT1 and PRRs (>10-fold) as compared to ChB16 or uB16, were only semipermissive to EHDV-TAU (failing to increase viral titer); uB16 cells, which expressed only ∼5-fold more of STAT1 or PRRs than ChB16 cells, were productively infected and killed by EHDV-TAU, albeit at lower efficiency than ChB16. The relatively high levels of EHDV-TAU-mediated killing of ISF cells may reflect strong activation of cell-death-inducing antiviral mechanisms; for example, PKR activity, which indeed restricts EHDV-TAU infection in this cell type. Moreover, the notions of the specificity of EHDV-TAU toward transformed/cancerous cells is further supported by the negligible expression of NS3 in primary murine skin fibroblasts (not shown) and by the lack of apparent deleterious health effects in EHDV-TAU-treated mice. Treatment with 5AC or selected HDAC inhibitors increased the constitutive expression of STAT1 and PRRs in ChB16 cells. 5AC-treated ChB16 cells also responded to EHDV-TAU with additional increases in these genes, which together with the regained activation of JAK/STAT demonstrated the 5AC-mediated restoration of IFN-based antiviral responses. However, while pretreatment with IFN-β was cytoprotective blocking viral oncolysis (similarly to Reference 22), 5AC allowed for EHDV-TAU-induced oncolysis of murine and human melanomas. The fact that epigenetic modifiers (5AC and HDAC inhibitors), that target different chromatin components, both enhance the expression of STAT1 and PRRs is consistent with direct epigenetic regulation of these genes. Indeed, epigenetic silencing of ISGs was reported to occur upon cellular immortalization,[46] a fact which may also support the partial susceptibility of ISF cells to EHDV-TAU. However, the increased expression of PRRs may also stem from indirect effects of the epigenetic modifiers. Thus, 5AC induces expression of endogenous retroviruses that activate antiviral responses,[47] and histone deacetylases regulate antiviral responses through mechanisms other than chromatin modification.[48] In accord with effects on expression of immune regulators, epigenetic modifiers were proposed as combination therapy agents for both oncolytic virotherapy[5,49] and immunotherapy.[47]

Despite the lack of interferon secretion and STAT1 activation in EHDV-TAU-infected ChB16 cells following, we observed enhanced secretion of immune-stimulatory chemokines (CXCL1, CXCL2 and CXCL10) in vitro; suggesting EHDV-TAU-mediated activation of STAT1-independent proinflammatory signaling. These chemokines attract immune cells[50] and their secretion is predicted to modify the tumor microenvironment. In immune-competent C57BL6 mice EHDV-TAU-induced viral oncolysis of both proximal and distal tumors, in accord with a role for antitumor immunity in EHDV-TAU-mediated oncolysis. Indeed, EHDV-TAU increased the intratumoral infiltration of CD8+ cytotoxic T-cells. Most importantly, EHDV-TAU significantly enhanced the survival of mice baring two tumors (of which only one received direct/intratumoral injection of EHDV-TAU).

We propose that STAT1 is an "anchor" of a signature associated with immune activation and/or the mounting of antiviral responses. Thus, STAT1-based signatures may serve as important guides for the choice of immunotherapies or oncolytic virotherapy. Our data support the oncolytic potential of EHDV-TAU and suggest its ability to exploit tumor-induced defects to STAT1-regulated cell autonomous immunity.

ACKNOWLEDGMENTS

This study was supported by grants from the Israel Science Foundation (1966/18; Marcelo Ehrlich), Israel Cancer Association (20200132; ME; through kind donation from Lois Pope, ICA-USA), Colton-Nadal Fund (Marcelo Ehrlich), SPARK initiative (Marcelo Ehrlich, Eran Bacharach), Emerson Collective Cancer Research Fund (Marcelo Ehrlich, Eran Bacharach, Isaac P. Witz) and by The Dr. Miriam and Sheldon G. Adelson Medical Research Foundation (Needham, MA) (IPW). We would like to acknowledge the assistance of Emie Gueheneuc (Artemie07) in design and execution of the graphical abstract figure. This figure was created using Servier Medical Art templates, which are licensed under a Creative Common Attribution 3.0 Generic License. http://smart.servier.com/.

CONFLICT OF INTEREST

Marcelo Ehrlich and Eran Bacharach are applicant of the provisional patent 2017048-00 US Provisional Patent Application No. 62/525289, EPIZOOTIC HEMORRHAGIC DISEASE VIRUS—TEL AVIV UNIVERSITY (EHDV-TAU): ONCOLYTIC VIRUS FOR TREATING CANCER. All other authors declare no conflict of interests.

DATA AVAILABILITY STATEMENT

The data that supports the findings of this study are available in the Supplementary Material of this article. Data employed in analysis is available at public databases and portals (https://www.cbioportal.org/, https://www.encodeproject.org/, https://xenabrowser.net/). Further information is available from the corresponding authors under request.

ETHICS STATEMENT

All experiments involving animals were approved by the TAU Institutional Animal Care and Use Committee. Mice (ranging from 8 to 15 weeks old) were used for experiments in accordance with institutional ethical guidelines.

ORCID

Isaac P. Witz https://orcid.org/0000-0002-0341-4343
Marcelo Ehrlich https://orcid.org/0000-0002-2352-1808

REFERENCES

1. McGranahan N, Swanton C. Clonal heterogeneity and tumor evolution: past, present, and the future. *Cell*. 2017;168:613-628.
2. Vesely MD, Schreiber RD. Cancer immunoediting: antigens, mechanisms, and implications to cancer immunotherapy. *Ann N Y Acad Sci*. 2013;1284:1-5.
3. Bubenik J. MHC class I down-regulation: tumour escape from immune surveillance? (Review). *Int J Oncol*. 2004;25:487-491.
4. Wang Y, Wang H, Yao H, Li C, Fang JY, Xu J. Regulation of PD-L1: emerging routes for targeting tumor immune evasion. *Front Pharmacol*. 2018;9:536.
5. Danziger O, Shai B, Sabo Y, Bacharach E, Ehrlich M. Combined genetic and epigenetic interferences with interferon signaling expose prostate cancer cells to viral infection. *Oncotarget*. 2016;7:52115-52134.
6. Zaretsky JM, Garcia-Diaz A, Shin DS, et al. Mutations associated with acquired resistance to PD-1 blockade in melanoma. *N Engl J Med*. 2016;375:819-829.
7. Randow F, MacMicking JD, James LC. Cellular self-defense: how cell-autonomous immunity protects against pathogens. *Science*. 2013;340:701-706.
8. Yan N, Chen ZJ. Intrinsic antiviral immunity. *Nat Immunol*. 2012;13:214-222.
9. Capobianchi MR, Uleri E, Caglioti C, Dolei A. Type I IFN family members: similarity, differences and interaction. *Cytokine Growth Factor Rev*. 2015;26:103-111.
10. Schneider WM, Chevillotte MD, Rice CM. Interferon-stimulated genes: a complex web of host defenses. *Annu Rev Immunol*. 2014;32:513-545.
11. Katlinskaya YV, Katlinski KV, Yu Q, et al. Suppression of type I interferon signaling overcomes oncogene-induced senescence and mediates melanoma development and progression. *Cell Rep*. 2016;15:171-180.
12. Osborn JL, Greer SF. Metastatic melanoma cells evade immune detection by silencing STAT1. *Int J Mol Sci*. 2015;16:4343-4361.
13. Huangfu WC, Qian J, Liu C, et al. Inflammatory signaling compromises cell responses to interferon alpha. *Oncogene*. 2012;31:161-172.
14. Gao J, Shi LZ, Zhao H, et al. Loss of IFN-gamma pathway genes in tumor cells as a mechanism of resistance to anti-CTLA-4 therapy. *Cell*. 2016;167:397-404.e9.
15. Ascierto PA, Kirkwood JM. Adjuvant therapy of melanoma with interferon: lessons of the past decade. *J Transl Med*. 2008;6:62.
16. Fisher PB, Prignoli DR, Hermo H Jr, Weinstein IB, Pestka S. Effects of combined treatment with interferon and mezerein on melanogenesis and growth in human melanoma cells. *J Interferon Res*. 1985;5:11-22.
17. Kang DC, Gopalkrishnan RV, Wu Q, Jankowsky E, Pyle AM, Fisher PB. Mda-5: an interferon-inducible putative RNA helicase with double-stranded RNA-dependent ATPase activity and melanoma growth-suppressive properties. *Proc Natl Acad Sci U S A*. 2002;99:637-642.
18. Kato H, Takeuchi O, Mikamo-Satoh E, et al. Length-dependent recognition of double-stranded ribonucleic acids by retinoic acid-inducible gene-I and melanoma differentiation-associated gene 5. *J Exp Med*. 2008;205:1601-1610.
19. Strong JE, Coffey MC, Tang D, Sabinin P, Lee PW. The molecular basis of viral oncolysis: usurpation of the Ras signaling pathway by reovirus. *EMBO J*. 1998;17:3351-3362.
20. Stojdl DF, Lichty BD, tenOever BR, et al. VSV strains with defects in their ability to shutdown innate immunity are potent systemic anti-cancer agents. *Cancer Cell*. 2003;4:263-275.
21. Barhoom S, Farrell I, Shai B, et al. Dicodon monitoring of protein synthesis (DiCoMPS) reveals levels of synthesis of a viral protein in single cells. *Nucleic Acids Res*. 2013;41:e177.
22. Danziger O, Pupko T, Bacharach E, Ehrlich M. Interleukin-6 and interferon-alpha signaling via JAK1-STAT differentially regulate oncolytic versus cytoprotective antiviral states. *Front Immunol*. 2018;9:94.
23. Ben Baruch B, Blacher E, Mantsur E, et al. Stromal CD38 regulates outgrowth of primary melanoma and generation of spontaneous metastasis. *Oncotarget*. 2018;9:31797-31811.
24. Porgador A, Feldman M, Eisenbach L. H-2Kb transfection of B16 melanoma cells results in reduced tumourigenicity and metastatic competence. *J Immunogenet*. 1989;16:291-303.
25. Berger W, Elbling L, Minai-Pour M, et al. Intrinsic MDR-1 gene and P-glycoprotein expression in human melanoma cell lines. *Int J Cancer*. 1994;59:717-723.

26. Cerami E, Gao J, Dogrusoz U, et al. The cBio cancer genomics portal: an open platform for exploring multidimensional cancer genomics data. *Cancer Discov*. 2012;2:401-404.
27. Goldman M, Craft B, Brooks AN, Zhu J, Haussler D. The UCSC Xena platform for cancer genomics data visualization and interpretation. *bioRxiv*. 2018;38:675-678.
28. Cancer Genome Atlas Network. Genomic classification of cutaneous melanoma. *Cell*. 2015;161:1681-1696.
29. ENCODE Project Consortium. An integrated encyclopedia of DNA elements in the human genome. *Nature*. 2012;489:57-74.
30. Thomas PD, Campbell MJ, Kejariwal A, et al. PANTHER: a library of protein families and subfamilies indexed by function. *Genome Res*. 2003;13:2129-2141.
31. Praetorius C, Grill C, Stacey SN, et al. A polymorphism in IRF4 affects human pigmentation through a tyrosinase-dependent MITF/TFAP2A pathway. *Cell*. 2013;155:1022-1033.
32. Johnson CW, Barth RF, Adams D, Holman B, Price JE, Sautins I. Phenotypic diversity of murine B16 melanoma detected by anti-B16 monoclonal antibodies. *Cancer Res*. 1987;47:1111-1117.
33. Neuditschko B, Janker L, Niederstaetter L, et al. The challenge of classifying metastatic cell properties by molecular profiling exemplified with cutaneous melanoma cells and their cerebral metastasis from patient derived mouse Xenografts. *Mol Cell Proteomics*. 2020;19:478-489.
34. Woods DM, Woan K, Cheng F, et al. The antimelanoma activity of the histone deacetylase inhibitor panobinostat (LBH589) is mediated by direct tumor cytotoxicity and increased tumor immunogenicity. *Melanoma Res*. 2013;23:341-348.
35. Russell SJ, Peng KW, Bell JC. Oncolytic virotherapy. *Nat Biotechnol*. 2012;30:658-670.
36. Bourgeois-Daigneault MC, Roy DG, Falls T, et al. Oncolytic vesicular stomatitis virus expressing interferon-gamma has enhanced therapeutic activity. *Mol Ther Oncolytics*. 2016;3:16001.
37. O'Shea JJ, Schwartz DM, Villarino AV, Gadina M, McInnes IB, Laurence A. The JAK-STAT pathway: impact on human disease and therapeutic intervention. *Annu Rev Med*. 2015;66:311-328.
38. Schoggins JW, Wilson SJ, Panis M, et al. A diverse range of gene products are effectors of the type I interferon antiviral response. *Nature*. 2011;472:481-485.
39. Chow KT, Jr MG, Loo Y-M. RIG-I and other RNA sensors in antiviral immunity. *Annu Rev Immunol*. 2018;36:667-694.
40. Besch R, Poeck H, Hohenauer T, et al. Proapoptotic signaling induced by RIG-I and MDA-5 results in type I interferon-independent apoptosis in human melanoma cells. *J Clin Invest*. 2009;119:2399-2411.
41. Duewell P, Steger A, Lohr H, et al. RIG-I-like helicases induce immunogenic cell death of pancreatic cancer cells and sensitize tumors toward killing by CD8(+) T cells. *Cell Death Differ*. 2014;21:1825-1837.
42. Heidegger S, Wintges A, Stritzke F, et al. RIG-I activation is critical for responsiveness to checkpoint blockade. *Sci Immunol*. 2019;39:eaau8943.
43. Ishizuka JJ, Manguso RT, Cheruiyot CK, et al. Loss of ADAR1 in tumours overcomes resistance to immune checkpoint blockade. *Nature*. 2019;565:43-48.
44. Loo YM, Fornek J, Crochet N, et al. Distinct RIG-I and MDA5 signaling by RNA viruses in innate immunity. *J Virol*. 2008;82:335-345.
45. Trujillo JA, Sweis RF, Bao R, Luke JJ. T cell-inflamed versus non-T cell-inflamed tumors: a conceptual framework for cancer immunotherapy drug development and combination therapy selection. *Cancer Immunol Res*. 2018;6:990-1000.
46. Kulaeva OI, Draghici S, Tang L, Kraniak JM, Land SJ, Tainsky MA. Epigenetic silencing of multiple interferon pathway genes after cellular immortalization. *Oncogene*. 2003;22:4118-4127.
47. Chiappinelli KB, Strissel PL, Desrichard A, et al. Inhibiting DNA methylation causes an interferon response in cancer via dsRNA including endogenous retroviruses. *Cell*. 2015;162:974-986.
48. Chang HM, Paulson M, Holko M, et al. Induction of interferon-stimulated gene expression and antiviral responses require protein deacetylase activity. *Proc Natl Acad Sci U S A*. 2004;101:9578-9583.
49. Forbes NE, Abdelbary H, Lupien M, Bell JC, Diallo JS. Exploiting tumor epigenetics to improve oncolytic virotherapy. *Front Genet*. 2013;4:184.
50. Sokol CL, Luster AD. The chemokine system in innate immunity. *Cold Spring Harb Perspect Biol*. 2015;7:a016303.

SUPPORTING INFORMATION

Additional supporting information may be found online in the Supporting Information section at the end of this article.

How to cite this article: Dellac S, Ben-Dov H, Raanan A, et al. Constitutive low expression of antiviral effectors sensitizes melanoma cells to a novel oncolytic virus. *Int. J. Cancer*. 2021; 148:2321–2334. https://doi.org/10.1002/ijc.33401